EPJ Web of Conferences **75**, 05011 (2014)
DOI: 10.1051/epjconf/20147505011

Deterioration of exchange bias in CoO-Co bilayers by the roughness of the ZnO substrates

D. Stamopoulos[a], M. Zeibekis, E. Manios, N. Boukos and D. Niarchos

Institute of Advanced Materials, Physicochemical Processes, Nanotechnology and Microsystems, National Center for Scientific Research 'Demokritos', 15310, Aghia Paraskevi, Greece

Abstract. The Exchange Bias (EB) effect is observed at the interface of Antiferromagnet/Ferromagnet (AF/FM) structures and depends on the interface roughness (IR). Until today, only low IR values, usually below 10 nm, have been investigated. Here we investigate an extended range of IR through controlling the surface roughness (SR) of the employed substrates. We employ CoO/Co bilayers (thickness within 10-60 nm), a classic AF/FM structure that exhibits intense EB. ZnO was employed as the substrate in both film and bulk forms, enabling us to vary the SR up to 840 nm. Our data reveal a strong relative decrease, ranging within 20-65%, of both the shift H_{shift}^{EB} and coercive H_c^{EB} fields upon increase of SR (IR), for both parallel and normal magnetic field-sample configurations. For the explanation of these findings we propose that in thin AF/FM structures deposited on rough substrates the local magnetization, $\mathbf{M_f}$ of the FM is 'locked' mainly in-layer due to shape anisotropy, thus it is forced to follow the morphologically rough landscape of the substrate. This imposes misalignment between $\mathbf{M_f}$, that is 'directionally random', and $\mathbf{H_{ex}}$, that is 'directionally oriented'. This weakens the biasing potential of $\mathbf{H_{ex}}$ on $\mathbf{M_f}$ and reduces the relative macroscopic parameters H_{shift}^{EB} amd H_c^{EB}.

1 Introduction

Exchange bias (EB) coupling [1] is primarily an interface effect observed in Antiferromagnet/Ferromagnet (AF/FM) structures that is used in a wide spectrum of applications of both technological and basic research interest [1]. Referring to technological applications, it is commonly used in FM/NM/FM and FM/IN/FM trilayers (where NM and IN stand for normal metal and insulator, respectively) to 'pin' the magnetization of the one outer FM layer. By using the EB effect in such structures the relative magnetization configuration (homo-parallel or anti-parallel) of the outer FM layers can be controlled. In this way, the magnetoresistance of the complete AF/FM/NM/FM and AF/FM/IN/FM structures can be switched between two distinct states, thus enabling the utilization of these structures in devices such as magnetic field sensors and memory units [2-5]. Regarding basic research, the EB effect can be used in investigations on hybrid structures between FM and superconducting (SC) constituents that are generally considered as incompatible since the exchange field of the FM is detrimental to the singlet pairing of electrons that is at play in conventional low-T_c SC. However, in recent years hybrid AF/FM/SC/FM trilayers have attracted much interest due to their interesting transport properties [6-9]. In brief, the critical current, j_c and the critical temperature, T_c of the SC interlayer can be controlled by the relative magnetization configuration of the outer FM layers, whether we refer to in-plane (superconducting spin valve effect based on the exchange fields) or out-of-plane (superconducting magnetoresistance effect based on the stray fields), in respect to the hybrid surface [7-9]. Recent experiments proved that the EB mechanism can be used to control the transverse magnetostatic coupling of the outer FM layers through controlling the stray fields that pierce the SC interlayer, thus ultimately controlling the transport properties of those hybrid structures [7-9].

All applications of the EB effect discussed above depend on the interface roughness (IR) between the FM layers and the NM, IN or SC interlayer, since increased IR can motivate out-of-plane magnetization processes that ultimately can promote the magnetostatic coupling of the outer FM layers through the interlayer whether it is NM, IN or SC [9-11]. Thus, investigations of the influence of the IR on the EB effect are of interest to reveal its contribution to each of these phenomena.

Up to now, many studies have focused on low IR, usually below 10 nm ([1] and references therein). Here we investigate an extended range of IR through controlling the surface roughness (SR) of the employed substrates. The study is conducted on CoO/Co bilayers, a well studied AF/FM model system that exhibits intense EB. Zinc oxide (ZnO) was employed as the substrate in both film and bulk forms, enabling us to vary the SR up to 840 nm.

[a] Corresponding author: densta@ims.demokritos.gr

2 Methods

ZnO substrates of variable SR (mean surface roughness denoted as $<S_a>$) were prepared in bulk (pellet) and layered (film) forms by means of sintering and e-beam evaporation on SiO_2 substrates, respectively. The SR of the ZnO bulk substrates was systematically varied through sintering. Starting powder (99.7% purity) was initially dry pressed in pellet form under 100 Tones for 2 minutes and was sintered at different temperatures for 12 hours in air. Obviously, by changing the SR of the substrate we vary the IR of the AF/FM bilayer, that is deposited on top.

Co films with thickness ranging within 10-60 nm were rf-sputtered at 30 Watt under $3x10^{-3}$ Torr of 99.999% pure Ar atmosphere on the ZnO substrates. The desired CoO AF layer was formed at the bottom part of the Co film during the deposition process through the absorption of O_2 originating from the ZnO substrates.

The SR was systematically estimated from Atomic Force Microscopy (AFM) data that were acquired by means of a scanning probe microscope Solver PRO [NT-MDT Co, Moscow, Russia] having a 100x100x5 μm^3 xyz-scanner hosted on an active vibration isolation table Halcyonics MOD-1M Plus [Halcyonics GmbH, Goettingen, Germany]. Our measurements were performed in the non-contact scanning mode with NCHR cantilevers that end to silicon nitride tips [Nano and More GmbH, Wetzlar, Germany] having the nominal parameters, spring constant=42 Nm^{-1} and resonance frequency=320 kHz. The optimum imaging results were obtained for scanning parameters: line frequency=1-2 Hz, area=0.5x0.5-50x50 μm^2 and lines per image=256-512.

Detailed magnetization data were obtained using a SQUID unit [Quantum Design, San Diego, CA, USA]. Both parallel and normal configurations of the external magnetic field, $\mathbf{H_{ex}}$ in respect to the sample surface were investigated. Referring to the EB mechanism both virgin and biased loops were obtained by cooling from room temperature under zero and a sufficiently high magnetic field, respectively.

3 Results and discussion

Figure 1 shows the dependence of the mean surface roughness, $<S_a>$ on the sintering temperature, T_{sin}. We see that the SR, as calculated from detailed AFM measurements (see figures 5(a)-5(c), below), exhibits an abrupt increase from $<S_a>$=120 nm at T_{sin}=800 ^oC to $<S_a>$=840 nm at T_{sin}=1400 ^oC. The respective value of a 200 nm thick ZnO films that were used as reference was $<S_a>$=33 nm (black circle in figure 1).

Since it is well known that the EB effect is strongly reduced upon increase of the FM layer thickness as $H_{shift}^{EB} \sim 1/d_{FM}$ [1] in this study we examined relatively thin Co films, with thickness ranging within 10-60 nm, aiming to preserve a noticeable effect even for the case of increased IR investigated here. We examined both the normal and parallel magnetic field-sample configurations.

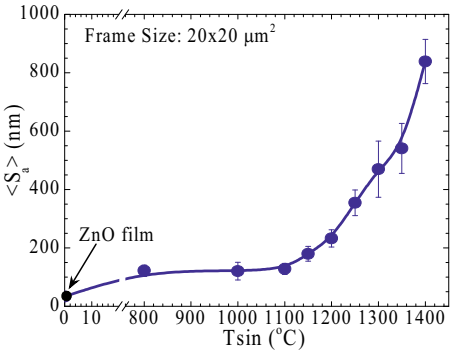

Fig. 1. Dependence of the mean surface roughness, $<S_a>$ on the sintering temperature, T_{sin} for as prepared ZnO bulk pellets. The black circle represents the mean surface roughness of a ZnO film of thickness 200 nm. The solid line is guide to the eye.

Figures 2(a) and 2(b) show representative isothermal magnetization loops at T=10 K, for the parallel magnetic field-sample configuration, for Co thickness of 10 nm and 60 nm, respectively. Both the virgin and biased states are presented for the ZnO-film substrate, while only the biased state is shown for the two ZnO-bulk substrates sintered at the lowest, T_{sin}=800 ^oC and highest, T_{sin}=1400 ^oC temperatures investigated here having the lowest, $<S_a>$=120 nm and highest, $<S_a>$=840 nm SR mean values, respectively.

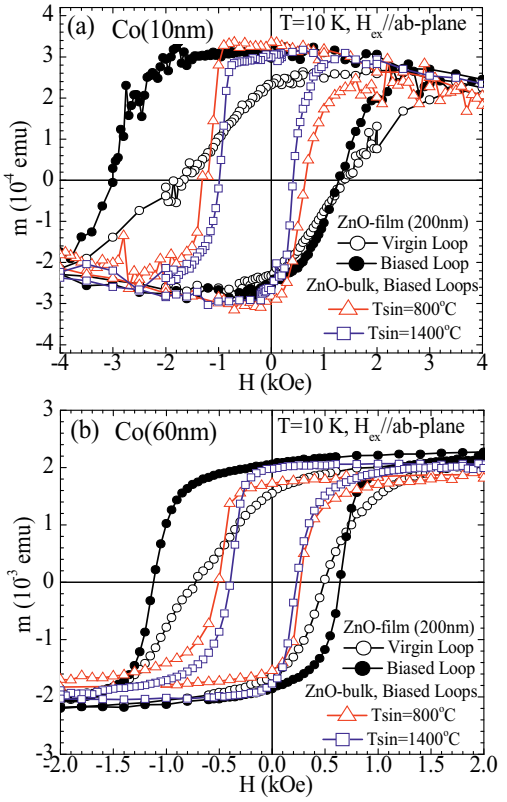

Fig. 2. Isothermal magnetization loops measured at T=10 K for the parallel magnetic field-sample configuration for Co thickness (a) 10 nm and (b) 60 nm. In both cases the virgin and biased loops are presented for the ZnO-film, while only the biased loops are shown for the ZnO-bulk sintered at T_{sin}=800 ^oC and T_{sin}=1400 ^oC.

By comparing the virgin and biased loops, a regular negative EB shift, H_{shift}^{EB} is observed, associated with the unidirectional magnetic anisotropy of the biased system in the opposite direction of the cooling field. Except for

the behavior of H_{shift}^{EB} we have also analyzed the respective variation of the coercive field, H_c^{EB}. From these data we see that both H_{shift}^{EB} and H_c^{EB} decrease with Co thickness, as expected [1] (note the different magnetic field range in figures 2(a) and 2(b)). In addition, both H_{shift}^{EB} and H_c^{EB} progressively decrease as the $<S_a>$ of the substrate (and the respective IR of the CoO/Co structure) increases. The magnetization data for the normal magnetic field-sample configuration are similar.

To quantify the influence of $<S_a>$ on these parameters we define the EB shift field as

$$H_{shift}^{EB}=-(H_{c-}+H_{c+})/2$$

and the EB coercive field as

$$H_c^{EB}=-(H_{c-}-H_{c+})/2$$

where H_{c-} and H_{c+} are the coercive fields defined from the descending and ascending branches of the magnetization loop, respectively.

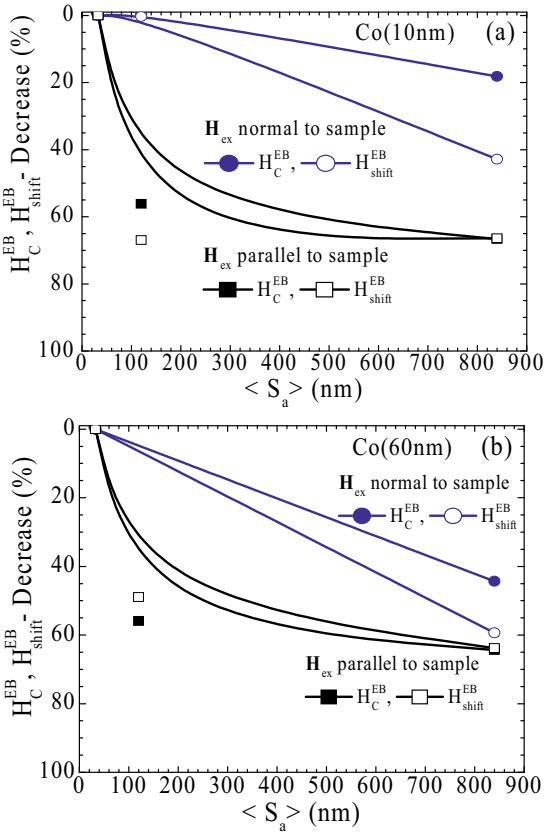

Fig. 3. Relative decrease of H_c^{EB} and H_{shift}^{EB} as a function of mean surface roughness, $<S_a>$ of the substrate for both parallel and normal magnetic field-sample configurations for Co thickness (a) 10 nm and (b) 60 nm. The solid lines are guide to the eye.

The results for both the parallel and normal magnetic field-sample configurations are summarized in figures 3(a) and 3(b) for the Co films of 10 nm and 60 nm, respectively. From these data we see a strong relative decrease of both H_{shift}^{EB} and H_c^{EB} with the increase of IR induced by the increased $<S_a>$ of the ZnO substrates, for both parallel and normal $\mathbf{H_{ex}}$. For the parallel magnetic field-sample configuration the relative decrease of both H_{shift}^{EB} and H_c^{EB} does not seem to depend on the Co thickness exhibiting a very similar value of almost 65% for the maximum $<S_a>$=840 nm. On the contrary, for the normal magnetic field-sample configuration the relative decrease of H_{shift}^{EB} is almost 45% for Co thickness of 10 nm, while it is noticeably higher, 60% for Co thickness of 60 nm. Referring to H_c^{EB} the relative decrease is almost 20% for Co thickness of 10 nm, while it is again noticeably higher, 45% for Co thickness of 60 nm.

For the interpretation of these data we propose a toy model based on the following assumption: the parts of CoO/Co bilayer deposited at the lateral surface of the ZnO grains experience the external magnetic field $\mathbf{H_{ex}}$ at randomly distributed directions, as illustrated in the cartoon of figure 4 for the side view line-section of a single ZnO grain.

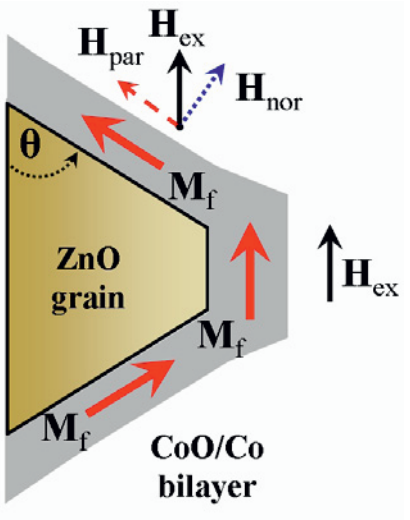

Fig. 4. The cartoon depicts, in side view, the misalignment observed between the local magnetization, $\mathbf{M_f}$ of the CoO/Co bilayer and the applied magnetic field, $\mathbf{H_{ex}}$ at the neighbourhood of a ZnO grain due to the rough landscape. The thin solid arrow is the external magnetic field, $\mathbf{H_{ex}}$. The thick solid arrows depict the magnetization, $\mathbf{M_f}$, that lies in-layer at the lateral sides of the ZnO grain. The dashed and dotted arrows represent the parallel and normal components of $\mathbf{H_{ex}}$ to the local magnetization, $\mathbf{M_f}$ of the CoO/Co bilayer, respectively. The scheme refers to the parallel magnetic field-sample configuration.

Obviously, the rougher the ZnO landscape, the more randomly distributed is the direction between the local magnetization $\mathbf{M_f}$ of the CoO/Co structure and the external magnetic field $\mathbf{H_{ex}}$. Referring to the ZnO substrates, representative AFM images of the surface landscape are shown in figures 5(a)-5(c) for ZnO-film (200 nm), and ZnO-bulk sintered at T_{sin}=800°C ($<S_a>$=120 nm) and T_{sin}=1400°C ($<S_a>$=840 nm), respectively.

The overall decrease of both H_{shift}^{EB} and H_c^{EB} upon increase of SR (IR) observed in both 10 nm and 60 nm thin Co films can be ascribed to the competition between the *intrinsic* mechanism of shape anisotropy that 'locks' $\mathbf{M_f}$ in-layer [12,13] and the *extrinsic* cause of the applied magnetic field $\mathbf{H_{ex}}$ that tries to bias $\mathbf{M_f}$ by rotating it along its direction. We propose that the key parameter for the decrease of both H_{shift}^{EB} and H_c^{EB} upon increase of SR (IR) observed in our data is the misalignment between $\mathbf{M_f}$ and $\mathbf{H_{ex}}$ due to the morphologically rough landscape of

the ZnO substrate as clearly illustrated by the AFM data presented in figures 5(a)-5(c), in top view. The overall concept is schematically illustrated in figure 4, in side view, for the parallel magnetic field-sample configuration; the parts of the CoO/Co bilayer that is deposited at the lateral surfaces of the ZnO grains possess a magnetization vector, $\mathbf{M_f}$ that since it is 'locked' in-layer due to the shape anisotropy [12,13], it experiences the external magnetic field $\mathbf{H_{ex}}$ at a misalignment angle θ. As a consequence, the biasing potential of $\mathbf{H_{ex}}$ is weakened due to its effectively smaller value $\mathbf{H_{ex}^{ef}}=\mathbf{H_{par}}=\mathbf{H_{ex}}\cos\theta$. Obviously, since the misalignment angle between $\mathbf{M_f}$, that is 'directionally random' and $\mathbf{H_{ex}}$, that is 'directionally oriented' increases with SR (IR), the biasing potential of $\mathbf{H_{ex}}$ on $\mathbf{M_f}$ should decrease. Thus, both relative macroscopic parameters H_{shift}^{EB} and H_c^{EB} should also decrease, as observed in our data. The same explanation can be applied for the normal magnetic field-sample configuration.

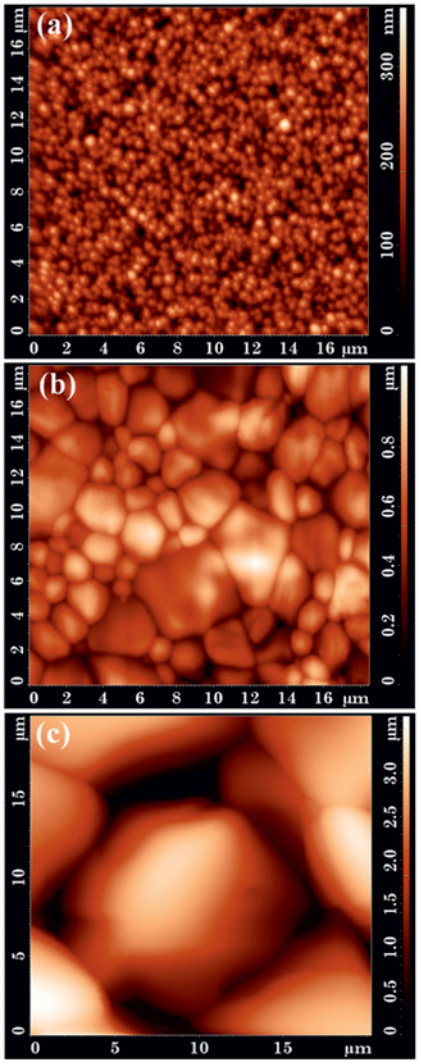

Fig. 5. Representative AFM images, in top view (20x20 μm^2), of ZnO (a) film and bulk sintered at (b) T_{sin}=800°C and (c) T_{sin}=1400°C.

Except for the issues discussed above additional mechanisms can be at play making the overall situation even more complicate. For instance, by using simple geometric arguments and algebraic calculations it is easy to show that the thickness of the deposited CoO/Co bilayer is strongly modulated by the rough landscape of the ZnO substrates; the nominal thickness, t_{nom} is only preserved at the areas that during the deposition are normal to the incident plasma, while at the lateral surfaces of the ZnO grains the effective thickness, t_{eff} is strongly reduced following a $t_{eff}=t_{nom}\cos\theta$ law, where θ is the angle shown in figure 4 that varies within 0° and 90°. The effective reduction of the Co thickness farther promotes the shape anisotropy mechanism, ultimately weakening the bias potential of the applied magnetic field. The theoretical investigation of this additional mechanism is in progress.

4 Conclusions

In thin CoO/Co bilayers deposited on rough ZnO substrates the magnetization, $\mathbf{M_f}$ of Co is 'locked' mainly in-layer due to shape anisotropy; thus, it is forced to follow the morphologically rough landscape of the ZnO substrate. As a consequence, misalignment is observed between $\mathbf{M_f}$, that is 'directionally random', and the biasing field $\mathbf{H_{ex}}$, that is 'directionally oriented'. This weakens the biasing potential of $\mathbf{H_{ex}}$ on $\mathbf{M_f}$ and reduces the relative macroscopic parameters H_{shift}^{EB} amd H_c^{EB}. The effect gets pronounced with the increase of SR (IR).

Acknowledgments

M. Zeibekis acknowledges the A.G. Leventis Foundation for support through a scholarship.

References

1. J. Nogues, I.K. Schuller, J. Magn. Magn. Mater. **192**, 203 (1999)
2. M.N. Baibich, J.M. Broto, A. Fert, F. Nguyen Van Dau, F. Petroff, Phys. Rev. Lett. **61**, 2472 (1988)
3. J. Daughton J. Brown, E. Chen, R. Beech, A. Pohm, W. Kude, IEEE Trans. Magn. **30**, 4608 (1994)
4. M. Dax, Semicond. Int. **20**, 84 (1997)
5. G.A. Prinz, Science **282**, 1660 (1998)
6. N.M. Nemes et al., Phys. Rev. B **81**, 024512 (2010)
7. D. Stamopoulos, E. Manios, M. Pissas, Supercond. Sci. Technol. **20**, 1205 (2007)
8. D. Stamopoulos, E. Manios, M. Pissas, Phys. Rev. B **75**, 014501 (2007)
9. D. Stamopoulos, E. Manios, M. Pissas, *Exchange Biased and Plain Superconducting Ferromagnetic Layered Hybrids* (Nova Science Publishers Inc, New York, USA, 2010)
10. B.D. Schrag et al., Appl. Phys. Lett. **77**, 2373 (2000)
11. S. Demokritov et al., Phys. Rev. B **49**, 720 (1994)
12. M. Hehn, S. Padovani, K. Ounadjela, J.P. Bucher, Phys. Rev. B **54**, 3428 (1996)
13. J. Brandenburg, R. Huhne, L. Shultz, V. Neu, Phys. Rev. B **79**, 054429 (2009)